

1 **Lessons on textile history and fibre durability**
2 **from a 4000-year-old Egyptian flax yarn**

3
4
5 **Authors:** Alessia Melelli¹, Darshil U. Shah², Gemala Hapsari³, Roberta Cortopassi⁴, Sylvie
6 Durand⁵, Olivier Arnould⁶, Vincent Placet³, Dominique Benazeth⁴, Johnny Beaugrand⁵, Frédéric
7 Jamme⁷, Alain Bourmaud^{1,*}.

8
9
10 ¹ Univ. Bretagne Sud, UMR CNRS 6027, IRDL, Lorient, France.

11 ²Centre for Natural Material Innovation, Department of Architecture, University of Cambridge,
12 Cambridge CB2 1PX, United Kingdom

13 ³FEMTO-ST Institute, Department of Applied Mechanics, UMR CNRS 6174, University of
14 Franche-Comté, 25000 Besançon, France

15 ⁴Musée du Louvre, Département des Antiquités Egyptiennes, 75058 Paris cedex 1, France.

16 ⁵INRAE, UR1268 BIA Biopolymères Interactions Assemblages, 44316 Nantes, France

17 ⁶LMGC, Université de Montpellier, UMR CNRS 5508, Montpellier, France

18 ⁷Synchrotron SOLEIL, DISCO beamline, Gif-sur-Yvette, France

19
20 *Correspondence to: alain.bourmaud@univ-ubs.fr

24 **Flax has a long and fascinating history. This plant was domesticated around 8,000 BCE¹,**
25 **in the Fertile Crescent area², first for its seeds and then for its fibres^{1,3}. Although, its uses**
26 **existed long before domestication - residues of flax yarn dated 30,000 years ago have**
27 **been found in the Caucasus area⁴. However, it is Ancient Egypt which laid the**
28 **foundations for the cultivation of flax as a textile fibre crop⁵. Today, flax fibres are used**
29 **in high-value textiles, as well as natural actuators⁶ or reinforcements in composite**
30 **materials⁷. Flax is therefore a bridge between ages and civilizations. For several decades,**
31 **the development of non- or micro-destructive analysis techniques has led to numerous**
32 **works on the conservation of ancient textiles. Non-destructive methods such as optical**
33 **microscopy⁸, or vibrational techniques^{9,10} have been largely used to investigate**
34 **archaeological textiles, principally to evaluate their degradation mechanisms and state of**
35 **conservation. Vibrational spectroscopy studies can now benefit from synchrotron**
36 **radiation¹¹ as well X-ray diffraction (XRD) measurement in the archaeometric study of**
37 **historical textiles^{12,13}. Conservation of mechanical performance and the ultrastructural**
38 **differences between ancient and modern flax varieties have not been examined thus far.**
39 **Here, in order to assess the quality and durability of ancient flax fibres and relate this to**
40 **their processing methods, we examine the morphological, ultrastructural and mechanical**
41 **characteristics of a yarn from an Egyptian mortuary linen, dating from the early Middle**
42 **Kingdom (Eleventh dynasty, ca. 2033 - 1963 BCE), and compare them against a modern**
43 **flax yarn. Advanced microscopy techniques, such as nano-tomography, multiphoton**
44 **excitation microscopy and atomic force microscopy were used. Our findings reveal the**
45 **cultural know-how of this ancient civilization in producing high-fineness fibres, as well**
46 **as the exceptional durability of flax, which is sometimes questioned, demonstrating their**
47 **potential as reinforcements in high-tech composites.**

48

49 The most beautiful fabric pieces of flax date from Ancient Egypt (Fig. 1), their highly-preserved
50 state a result of their optimal conservation over millennia in coffins or tombs with remarkably
51 stable moisture and thermal conditions, as well as sheltering from UV light. Flax textiles were
52 particularly prized by the Egyptians because of its comfort and the fineness of its fibres¹⁴. Flax
53 was widely used for clothing (Fig 1.a) and in the fishing sector for work clothes, felucca sails and
54 nets. The funerary uses included mummy strips (Fig 1.b), funeral linen (Fig 1.c, d, g) as well as
55 ornaments (Fig 1.e).

56 In terms of cultivation, the fertile Nile valley with its light and rich or sandy soils was particularly
57 suitable for flax. After growing, the stems were pulled out, as shown in illustrations found in the
58 tomb of Sennedjem (Deir el Medineh, Egypt) and then probably water-retted. Over the past
59 century or so, growth conditions have changed and varietal selection has significantly increased
60 the crop's fibre yields¹⁵. It is therefore difficult to compare varieties across the ages. Even so, an
61 in-depth study of 407 flax genotypes of different origins has shown that regions that have been
62 the centre of origin of the crop, such as the Mediterranean or Abyssinia, highlight haplotypes
63 that are more unique than the temperate group and are representative of oil-seed plants¹⁶.

64 According to Braun¹⁷, the flax found in the lake dwelling does not belong to the species now
65 cultivated (*Linum usitatissimum* L) but to the *Linum angustifolium* which is not cultivated at the
66 present time. Today's cultivated flax *Linum usitatissimum* L. is considered as being
67 domesticated from the wild progenitor pale flax *Linum angustifolium* Huds. Both have
68 phenotypic characters of great heritability, and are distinguishable by several characteristics,
69 such as the length and width of petals, size of seeds, colour and shape of the flower, height of
70 plants but also the number of days until emergence from the soil or flowering¹⁸. However, the
71 height of the plants shown on the Egyptian bas-reliefs¹⁹ as well as the size of the seeds found
72 during excavation¹ suggests that the species cultivated by the Egyptians were morphologically
73 close to those we know today.

74 Figures 2.a and 2.d compare the overall architecture, observed by SEM, of old (Fig. 1.g and
75 Supplementary Fig.1.a) and modern (Supplementary Fig.1.b) flax yarn, respectively. Despite a
76 lower level of twist (about 180 turns per metre (tpm) against 320 tpm for the modern flax), the
77 old flax possesses a similar metric number (about 122 tex or 8.2 km/kg), showing the mastery of
78 the Egyptians in manual spinning. Figure 2.b reveals the level of individualisation of the fibres.
79 In the flax stem, fibres are aggregated in cohesive bundles made of several tens of fibres, the
80 latter being more or less divided after retting and extraction stages. The old yarn is mainly made
81 up of elementary flax fibres; the residues of cortical parenchyma and middle lamellae are very
82 few. This demonstrates the effectiveness of the water-retting process utilized at the time as
83 Pliny the Elder explained²⁰. Water-retting enables homogeneous retting and, when it is well
84 executed, enables the production of very fine fibres. One can notice that the low fibre yield in
85 ancient flax varieties can also lead to easier retting and fibre division²¹. In modern flax fibre
86 extraction processes, stems undergo field retting over several weeks. Dependent on natural
87 weather conditions, this can lead to retting heterogeneity. As a consequence, numerous
88 residues of pectic intermediate lamellae or cortical parenchyma are visible on the modern flax
89 yarn (Fig. 2.e, h). Such residues increase roughness of the yarn and are detrimental to the
90 sensation of comfort (e.g. softness). This is in contrast to the reputation of Egyptian flax fabrics,
91 whose most beautiful specimens were reserved for members of high society. These
92 observations validate the important know-how of ancient Egyptians in textile manufacturing. The
93 scanning electron micrographs (Figs. 2.a, b) also reveal the excellent general conservation of
94 the ancient fibrous yarns.

95 Figures 2.g and 2.h present cross-sections of the old and modern yarn observed in nano-
96 tomography and Figure 2.i illustrates the analysed distribution in elementary fibre diameters for
97 the two materials. The mean diameters are $14.3 \pm 3.3 \mu\text{m}$ for the fibres in the old yarn ($n = 523$)
98 and $17.6 \pm 3.6 \mu\text{m}$ for the modern yarn ($n = 208$); both diameter values are consistent with

99 typically reported values on flax fibres²². A significant difference in elementary fibre diameters is
100 observed and confirmed by a student test with $P \leq 0.001$. The smaller diameters of old flax may
101 be related to the plant variety, the weather conditions during growth (hydraulic stress, for
102 example)²³, and/or even the sampling area within the stem, with larger diameter fibres being
103 generally located in the middle section of the stem height²⁴. The retting method utilized may also
104 explain the differences and scatter in elementary fibre diameters between the old and modern
105 flax yarn (Fig. 2.i). The use of water-retting for the old flax yarn, leads to completely separated
106 fibres and free from surface residues (Fig. 2.b). This further demonstrates the skill of the ancient
107 Egyptians in obtaining fine yarns and textiles.

108 Differences are also visible in the size of the lumens, with SEM and tomographic images
109 (Fig. 2.c, f, g and h) showing larger ones for old flax fibres. While the lumens of modern flax
110 fibres represent only a few percent of the total surface area²⁵, here, old fibres possess lumens
111 of the order of 30-40%, comparable to wood or coconut fibres²⁵. We hypothesize that these low
112 wall thicknesses of old flax may be due to a premature halt in the cellulose filling process of the
113 cell walls following the intrusive growth phase²⁴. This filling can be interrupted by extreme
114 weather conditions, such as lodging or marked periods of hydraulic stress²⁶.

115 Flax fibres are characterised by their multi-layered structure and their generally polygonal
116 shape, as well as by the presence of structural defects known as kink-bands²⁷, distributed along
117 the fibre length. Notably, the relative quantity and size of these kink-bands is particularly large
118 on old fibres (Fig. 2.b, Fig. 3.a, b) in comparison to modern fibres (Fig. 3.d, e). The origin of
119 these defects is not well known but the plant fibre community generally attributes them to
120 mechanical stresses induced during the extraction or processing of the stems, but also to
121 residual stresses that may be released during periods of stem or fibre drying, possibly during
122 the retting stage^{27,28}. The large quantity of kink-bands on old flax fibres may be the result of
123 aggressive decortication, scutching or spinning processes used by the Egyptians following

124 water-retting, but may also be caused by progressive release of internal stresses over the 4
125 millennia. In flax fibres, kink-bands modify the aesthetics and regularity of the fibres, and are
126 also considered as zones of weakness, especially when utilized in a fibre-reinforced
127 composite²⁹. Kink-bands also make the fibre more susceptible and sensitive to ageing by acting
128 as entry points for microorganisms or moisture to access the inner layers of the cell walls³⁰.

129 We specifically examined the kink-bands through multiphoton microscopy with second harmonic
130 generation imaging, which highlights crystalline cellulose within the plant cell walls. Figure 3.c
131 shows discontinuity and disorganization of crystalline cellulose in the kink-band of old flax, and
132 possibly indicate areas of low crystallinity in this region. Both these factors would cause kink-
133 band rich ancient flax fibres to be more brittle¹³. Indeed, these old fibres have proved to be very
134 fragile during handling, and impossible to isolate without breaking/damaging them for any
135 single-fibre tensile testing.

136 Finally, atomic force microscopy tests in peak force quantitative nano-mechanical (AFM-PF-
137 QNM) mode were conducted on transverse cross sections of old and modern flax fibres. Such
138 measurements (Fig. 4) allow estimation of the indentation modulus of flax plant cell walls, i.e.,
139 do not depend on the relative lumen size and are a useful measure for highlighting mechanical
140 property gradients or heterogeneities within cell walls³¹. Interestingly, we found that the AFM
141 mechanical properties are slightly higher for cell walls of old flax than those of modern flax, i.e.,
142 23.7 ± 0.2 GPa and 20.3 ± 0.1 GPa, respectively; for each batch, 2,500 indentation moduli
143 values were statistically compared and the student t-test confirmed that the two sets of moduli
144 are different with $P \leq 0.001$. Values of modern flax are in line with the measurements in the
145 literature²⁵ and measured by nanoindentation (Supplementary Tab.1). Measurements by
146 infrared spectroscopy (Supplementary Fig. 6 and Supplementary Tab.2) revealed a lower
147 intensity of peaks attributed to parietal hemicelluloses for old flax. It has been shown that the
148 longitudinal and transverse shear moduli of the fibres³² and especially the stiffness of the non-

149 cellulosic matrix of the plant cell walls³³ have a major effect on the indentation modulus; our
150 results confirm this important influence of hemicelluloses, even though they are the softest
151 component of the cell wall, on the indentation modulus. Higher indentation modulus has
152 previously been recorded on old wood samples and is attributed to a loss of pectins, as well as
153 modification of the ligno-cellulosic cell wall polymers³⁴. The wider literature supports the
154 hypothesis of a significant evolution in the ageing sensitive hemicellulosic polymers over 4,000
155 years. Differences in crystallinity were also checked through both nuclear magnetic resonance
156 (NMR) and X-Ray diffraction (XRD) measurements; Supplementary Figure 7 shows that the
157 cellulose crystallinity measured by both NMR (58.0% for Egyptian yarn and 56.0% for the
158 modern yarn) and XRD (59.6% for Egyptian yarn and 58.4% for the modern yarn) techniques is
159 comparable between the ancient and modern flax yarns. Moreover, the measured indentation
160 moduli are homogeneous in the fibre sections and show little dispersion, suggesting no ageing
161 gradient across a fibre transverse section. Such quantitative nano-structural measurements,
162 never before conducted on such ancient fibres, reveal the durability of these flax plant cell walls.
163 Even though at the fibre-scale, the kink-bands are regions of pronounced damage, the cell walls
164 themselves exhibit a moderate change in their elastic performance despite their age; only a
165 slight increase in their stiffness, connected to the evolution of their non-cellulosic polysaccharide
166 composition, is demonstrated.

167 Our structural examination of 4000-year old Egyptian flax fibres in comparison to modern flax
168 fibres has offered a number of insights on the textile know-how of the Egyptians, as well as on
169 the temporal evolution of flax fibres. Through water retting and manual processing, the ancient
170 Egyptians could separate the flax into very fine fibre bundles and in most cases even into single
171 fibres to make soft and luxurious quality textiles despite fully-manual processing. Local
172 nanomechanical measurements show an increase in cell wall stiffness of old fibres, probably
173 induced by the alteration of non-cellulosic polymers, as cellulose retained a crystallinity close to

174 that of contemporary fibres. In addition, a larger presence of structural defects – stress-
175 concentrating kink-bands with low cellulose crystallinity – is notable on the old, fragile fibres. In
176 future and in work-in-progress, we aim to go further by exploring the microfibrils angle (MFA)
177 values of ancient flax (through single fibre XRD and SHG), the internal structure of kink-bands
178 (by nanotomography) and if possible, to gain information on the Linum used by ancient
179 Egyptians thanks to genetic analysis. To improve durability at the fibre scale, producing fibres
180 with low quantities of defects is necessary, in particular if they are to be used as reinforcements
181 of next-generation environmentally-friendly composite materials. Intriguingly, the ancient
182 Egyptians had also dabbled their hands in making the first linen/plaster cartonnage
183 biocomposites for death masks, a number of which survive to date (Fig. 1.b).

184

185

186 **Methods**

187 Materials

188 Two samples of flax yarns were studied (Supplementary Fig. 1), an ancient and a
189 contemporary sample, referred to as old and modern flax, respectively, in the manuscript. The
190 large linen tabby, bordered with a fringe (inv. E 13595, Supplementary Fig. 1.a) was given in
191 1929 by Georges Daressy, former General Secretary of the Antiquity Service in Egypt, to the
192 Louvre Museum (Paris, France). Its provenance is unknown but this piece of shroud most likely
193 came from a tomb, because all the textiles of ancient Egypt were found in cemeteries. These
194 cemeteries were located in the desert in order to ensure dryness and optimal conservation of
195 the burials. Indeed, in the valley, the annual flooding of the Nile was too risky. Thus, the
196 Egyptian climate of the desert areas, which was exceptionally dry and favourable to the proper
197 conservation of organic materials, made it possible to find many fabrics in excellent condition.
198 The linen was radiocarbon dated in 2009 (Laboratoire de Mesure du Carbone 14, CEA-Saclay,

199 Gif-sur-Yvette Cedex, France): it had been harvested between 2140 and 1976 BC (with 95.4%
200 probability), during the 9th, 10th or 11th dynasties, a period known as the First Intermediate
201 Period and the beginning of the Middle Egyptian Kingdom. Morphological characteristics of the
202 ancient yarn were calculated from mass measurements and from image analysis. The linear
203 density and twist of this old yarn are 122 tex and 180 tpm, respectively. In addition, a
204 contemporary yarn was used (Supplementary Fig. 1.b). It was produced from textile flax (Melina
205 variety) cultivated in 2018 in Normandy (France) by Teillage Saint-Martin company; this flax was
206 dew-retted conventionally over 6 weeks and then scutched and hackled (Bourmaud et al. 2018
207 PMS). Then, it was wet spun by Safilin Pionki (Poland) with a linear density and twist of 105 tex
208 and 320 tpm, respectively.

209

210 SEM observations

211 For each of the two yarns, a sample of a few millimetres was used. A Jeol JSM 6460LV
212 scanning electron microscope was used to analyse the flax yarns; secondary emission electrons
213 were used, and the accelerating voltage was 3.0 kV. They were glued to a sample holder using
214 a conductive adhesive and then metallized with a thin layer of gold using an Edwards Scancoat
215 Six device for 180 s.

216

217 Multiphoton microscopy

218 *Preparation of samples*

219 An elementary fibre was extracted from the modern flax yarn and mounted on paper
220 support commonly used for tensile tests according to ASTM C1557 and fixed with universal
221 glue. The sample prepared was placed between two coverslips and scanned. In contrast, the
222 preservation state of the Egyptian yarn does not allow to extract elementary fibres, which are
223 more brittle, so a whole collective of less than 1 cm was mounted on paper support commonly
224 used for tensile tests but glued in the horizontal direction in order to use the aperture of 5 mm.

225 The sample prepared was placed between two coverslips and scanned by the multiphoton
226 microscope. The samples were mounted at 90° to the initial laser polarization position.

227 *Second harmonic generation (SHG) microscopy imaging*

228 SHG imaging was performed with a multiphoton Nikon A1 MP+ microscope (NIKON,
229 France) equipped with a long working distance (LWD) 16x (NA 0.80) water immersion objective
230 (NIKON, France). The system is equipped with a tuneable Mai Tai XF mode-locked Ti:sapphire
231 femtosecond laser (SPECTRA PHYSICS, France) and a half-wave plate (MKS-Newport, USA)
232 in front of the laser excitation beam. The half-wave plate was rotated to change the laser
233 polarisation angle until to reach the maximum intensity SHG signal of both flax yarns (maximum
234 signal reached 2°-3°). The excitation wavelength chosen was 810 nm (average power at 1.5 W)
235 to obtain the maximum of the performance from the filters equipped (SH collected with a
236 bandpass filter at 406/15 nm), and the maximum laser power percentage used was 2% for the
237 Egypt yarn and 5% for the modern yarn to avoid the bleaching of the surface. We collected both
238 autofluorescence and SHG signals by GaAsP NDD (gallium arsenide non-descanned)
239 detectors. The scan line average was 16, the scan velocity was fixed at 1 (fps) and the scan
240 size was 512x512pixels. All the measurements were performed at room temperature and dry
241 ambient.

242

243 X-ray tomography measurements

244 The yarns' microstructure was characterized using X-ray nanotomography. Image
245 acquisition was realized on an EasyTom RX Solutions micro/nano tomograph (RX Solutions,
246 Chavanod, France). A Lanthanum hexaboride (LaB6) filament was used as cathode with a
247 voltage of 50 keV and a current of 100 µA, leading to a resolution of 0.5 µm. The anode was in
248 beryllium and has a thickness of 0.5 mm. Resolution of the micro-CT images was set to 4.44
249 µm/pixel. The imager used was a Fluoroscopic High Speed imaging sub-system PaxScan

250 2520DX and the scintillator was produced with a direct deposition of Cesium Iodide (CsI). To
251 obtain optimum measurement contrast, the framerate has been set to 0.25 fps. In addition, in
252 order to minimize the measurement noise, each projection obtained was the result of the
253 averaging of 15 acquisitions. Finally, in order to obtain the most faithful reconstruction possible,
254 the flax fibers were measured in 1440 different positions (angles). The yarn centering was
255 carried out using a perforated carbon tube. The tube outside diameter was 1 mm and the inside
256 hole diameter was 0.5 mm. A little bit of glue was used to maintain the yarns. The measured
257 volume was 0.5 mm in diameter over a height of 0.8 mm with a resolution of 500 nm. In order to
258 allow maximum beam stability from the start of the measurement, the wire was preheated 3
259 hours before the start of the measurement. In total, each measurement therefore lasted
260 approximately 27 hours. An X-ray radiograph is given in Supplementary Fig. 2.a to illustrate the
261 measurement (the yarn is hardly perceptible). The reconstruction was carried out using Xact
262 software using the filtered back-projection method. For the noise filtering, the apodization was
263 done using a sine window with a threshold of 75% for the low pass filter. For the border filter a
264 Tukey window type was used with a non-filtered area of 46%. For more information on filters
265 and the effects of reconstruction filter on CBCT image quality see³⁵. Once the reconstruction
266 has been carried out, the result is stored in the form of a slices stack. An illustration is given
267 Supplementary Fig. 2.b. Finally, the analyses and reconstruction of surfaces were carried out
268 using the VGSTUDIO MAX software as illustrated on Supplementary Figs. 3.a and 3.b at two
269 different scales.

270

271 Nano-mechanical investigations

272 *Preparation of samples*

273 A subsample of less than 1 cm was cut from the ancient flax yarn (Louvre) and modern flax
274 yarn samples. The two subsamples were put in an oven at 60°C for two hours and then
275 embedded in Agar resin (epoxy resin Agar Low Viscosity Resin (LV) -Agar scientific UK). The

276 blocks prepared were put back in the oven at 60°C overnight for the final polymerisation of the
277 resin, then machined, to reduce their cross-section, and glued on a 12 mm AFM stainless steel
278 mounting disk. The sample surface was thus cut using an ultramicrotome (Ultracut S, Leica
279 Microsystems SAS, France) equipped with diamond knives (Histo and Ultra AFM, Diatome,
280 Switzerland) to obtain thin sections (about 50 nm thick in the last step) at reduced cutting speed
281 (~1 mm/s) to minimize compression and sample deformation during the cutting process, and
282 thus reduce the sample surface damage and topography (Supplementary Fig. 4).

283 *AFM PF-QNM investigations*

284 A Multimode 8 Atomic Force Microscope (Bruker, Billerica, Massachusetts, USA) was
285 equipped with a RTESPA-525 probe (Bruker probes, Billerica, Massachusetts USA) with a
286 nominal spring constant of 200 N/m and a resonance frequency of 525 kHz. The actual spring
287 constant was calculated with the Sader Method (<https://sadermethod.org/>). The AFM set-up was
288 calibrated with the relative method using sapphire as hard standard material to calculate the
289 deflection sensitivity and the PF-QNM synchronisation distance. A sample of aramid fibres K305
290 Kevlar Taffetas 305 g/m² (Sicommin epoxy systems-France) accurately prepared in blocks of
291 Agar resin (Agar Low Viscosity Resin (LV)-Agar scientific, UK), whose surface was prepared
292 with the same protocol as the flax samples, was previously tested by nanoindentation and then
293 used to calibrate the tip radius (aramid fibre ~24.3 GPa and embedded resin ~5.4 GPa). The
294 range of the stiffness of the cantilevers used was between 109 and 161 N/m and the tip radius
295 between 15 and 30 nm at the beginning of the measurements.

296 The fast scan axis angle was at 90°, the maximum of the peak force setpoint used was
297 200 nN, the oscillation frequency selected at 2 kHz, the Poisson's ratio used was set to 0 as the
298 tested cell walls are anisotropic, thus the modulus measured is the indentation modulus. The
299 maximum fast scan velocity was selected at 8 µm/sec and the image resolution set to 512x512
300 pixels. The gain was set in automatic mode.

301 Two to three different areas of each sample (old and modern respectively) were measured
302 to obtain a better statistic but only one representative area for each sample is reported in this
303 paper (Fig. 4, Supplementary Figs. 4 and 5). Supplementary Figure 4 shows the topography
304 images corresponding to investigated areas of Figure 4. To obtain the indentation modulus
305 values, the entire surface of the secondary S₂ (or G) wall of each fibre was selected; indentation
306 modulus data were automatically calculated for each point from the force-distance curves with a
307 DMT contact model using NanoScope Analysis software (Bruker, Billerica, Massachusetts,
308 USA).

309 Consequently, for each sample, the indentation modulus calculated were obtained from
310 two or three separate images and from between 80,000 and 140,000 points for each image
311 analysed using Gwyddion free software (<http://gwyddion.net/>). Figure 9 shows the calculation
312 mask, covering the investigated area for fibres of Figure 4. For each sample, histograms of
313 Figure 4 represent the data obtained from all the images analysed; 206,613 and 364,575 AFM
314 force curves were used for old and modern flax indentation modulus calculation, respectively.

315

316 Statistical analysis

317 A t-test was performed to quantify the statistical differences in fibre diameters and
318 indentation moduli values between the old and modern fibres. P value was calculated for the
319 two cases, with significance level $\alpha = 0.05$.

320

321

322

323 **Acknowledgements**

324 VP and GH sincerely thank Dr. Pierrick Malécot and the MIFHySTO research platform
325 (FEMTO-ST, UTINAM and ICB institutes) at Université Bourgogne Franche-Comté (UBFC) for
326 the technical and scientific support provided for nanotomography experiments; Xavier Falourd
327 and Loïc Foucat (INRAE) are also thanked for NMR investigations. The authors want to thank
328 the INTERREG IV Cross Channel programme for funding this work through the FLOWER
329 project (Grant number n°23). SOLEIL Synchrotron is also thanked for funding the 99180266 and
330 99200015 in-house proposals. This work has also been supported by the EIPHI Graduate
331 school (contract "ANR-17-EURE-0002").

332

333

334 **Author contributions**

335 A.B. and D.U.S designed this work. A.M., G.H., O.A., S.D., V.P., J.B., F.J. and A.B.
336 collected and analyzed data. A.B., A.M. and D.U.S wrote and revised the paper with
337 contributions from G.H., R.C., O.A., V.P., D.B., S.D., J.B. and F.J.

338

339 **Competing interests statement**

340 The authors declare no competing interests.

341

342 **Data availability**

343 The data that supports the plots within this paper and the findings of this work are available
344 from the corresponding author on reasonable request.

345

346 **Code availability**

347 The open-source and commercial software used for data analysis are referenced in the
348 Methods section.

349

350

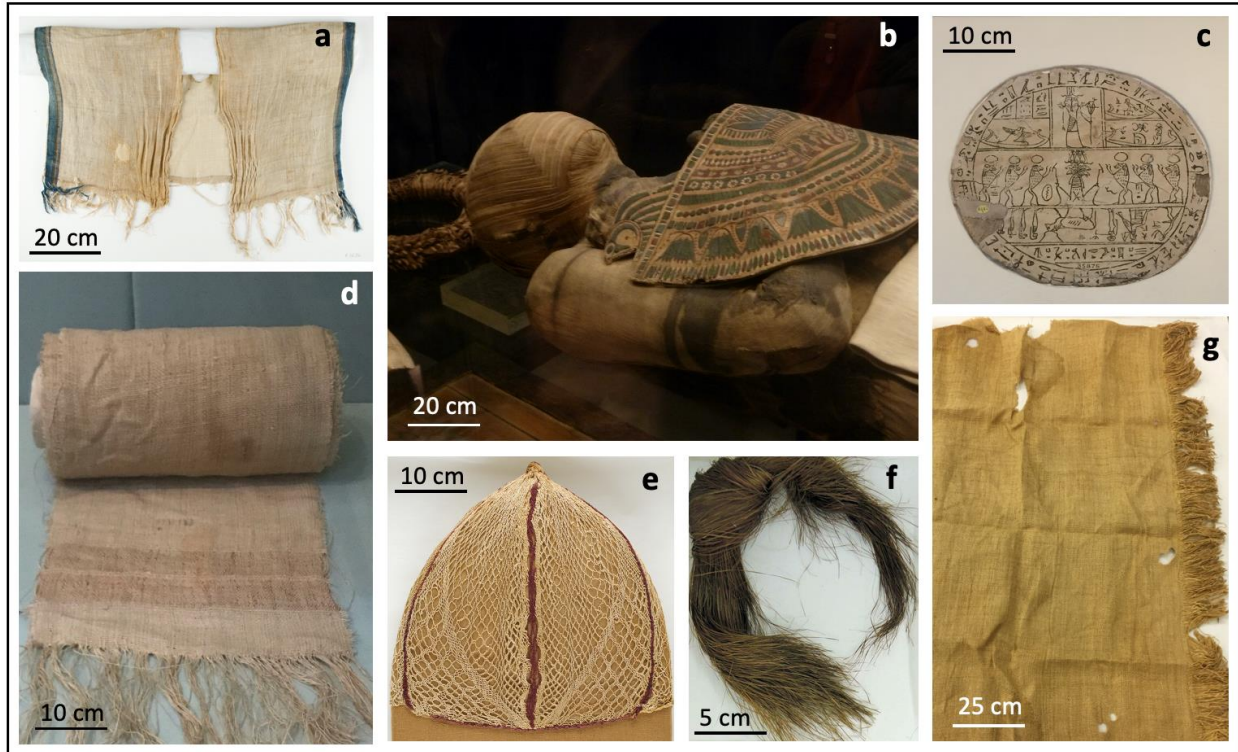
351 **References**

- 352 1. Van Zeist, W. & Bakker-Heeres, J. A. H. Evidence for linseed cultivation before 6000 bc.
353 *J. Archaeol. Sci.* **2**, 215–219 (1975).
- 354 2. Hopf, M. Plant remains and early farming in Jericho 1. in *The Domestication and*
355 *Exploitation of Plants and Animals*. (ed. Dibbleby, G.) (2008).
- 356 3. Herbig, C. & Maier, U. Flax for oil or fibre? Morphometric analysis of flax seeds and new
357 aspects of flax cultivation in Late Neolithic wetland settlements in southwest Germany.
358 *Veg. Hist. Archaeobot.* **20**, 527 (2011).
- 359 4. Kvavadze, E. *et al.* 30,000-Year-Old Wild Flax Fibers. *Science (80-.)*. **325**, 1359 (2009).
- 360 5. Heer, O. Prehistoric culture of flax. *Nature* 453 (1873).
- 361 6. Le Duigou, A. & Castro, M. Evaluation of force generation mechanisms in natural,
362 passive hydraulic actuators. *Sci. Rep.* **6**, 18105 (2016).
- 363 7. Mohanty, A. K., Vivekanandhan, S., Pin, J.-M. & Misra, M. Composites from renewable
364 and sustainable resources: Challenges and innovations. *Science (80-.)*. **362**, 536–542
365 (2018).
- 366 8. Bruni, S. *et al.* Analysis of an archaeological linen cloth: The shroud of Arquata. *Radiat.*
367 *Phys. Chem.* **167**, 108248 (2020).
- 368 9. Edwards, H. G. M., Ellis, E., Farwell, D. W. & Janaway, R. C. Preliminary Study of the
369 Application of Fourier Transform Raman Spectroscopy to the Analysis of Degraded

- 370 Archaeological Linen Textiles. *J. Raman Spectrosc.* **27**, 663–669 (1996).
- 371 10. Kavkler, K., Gunde-Cimerman, N., Zalar, P. & Demšar, A. FTIR spectroscopy of
372 biodegraded historical textiles. *Polym. Degrad. Stab.* **96**, 574–580 (2011).
- 373 11. Kavkler, K., Šmit, Ž., Jezeršek, D., Eichert, D. & Demšar, A. Investigation of
374 biodeteriorated historical textiles by conventional and synchrotron radiation FTIR
375 spectroscopy. *Polym. Degrad. Stab.* **96**, 1081–1086 (2011).
- 376 12. Müller, M. *et al.* Identification of ancient textile fibres from Khirbet Qumran caves using
377 synchrotron radiation microbeam diffraction. *Spectrochim. Acta Part B At. Spectrosc.* **59**,
378 1669–1674 (2004).
- 379 13. Herrera, L. K. *et al.* Identification of cellulose fibres belonging to Spanish cultural heritage
380 using synchrotron high resolution X-ray diffraction. *Appl. Phys. A* **99**, 391–398 (2010).
- 381 14. Weiss, E. & Zohary, D. The Neolithic Southwest Asian Founder Crops: Their Biology and
382 Archaeobotany. *Curr. Anthropol.* **52**, S237–S254 (2011).
- 383 15. Botany of Flax. *Nature* **170**, 557–559 (1952).
- 384 16. Sertse, D., You, F. M., Ravichandran, S. & Cloutier, S. The genetic structure of flax
385 illustrates environmental and anthropogenic selections that gave rise to its eco-
386 geographical adaptation. *Mol. Phylogenet. Evol.* **137**, 22–32 (2019).
- 387 17. Braun, A. Plants of Ancient Egypt. *Sci. Am.* **173**, 2760 (1879).
- 388 18. Diederichsen, A. & Hammer, K. Variation of cultivated flax (*Linum usitatissimum* L.
389 subsp. *usitatissimum*) and its wild progenitor pale flax (subsp. *angustifolium* (Huds.)
390 Thell.). *Genet. Resour. Crop Evol.* **42**, 263–272 (1995).
- 391 19. Kawami, T. S. A Craft in Antiquity. *Science (80-)*. **256**, 1065–1066 (1992).
- 392 20. André, J. Nature du lin et horticulture. in *Pline l’Ancien, Histoire naturelle* (ed. Budé)
393 (1964).
- 394 21. Goudenhoft, C., Bourmaud, A. & Baley, C. Varietal selection of flax over time: Evolution
395 of plant architecture related to influence on the mechanical properties of fibers. *Ind. Crops*

- 396 *Prod.* **97**, 56–64 (2017).
- 397 22. Baley, C. & Bourmaud, A. Average tensile properties of French elementary flax fibers.
398 *Mater. Lett.* **122**, 159–161 (2014).
- 399 23. Chemikosova, S. B., Pavlencheva, N. V, Gur'yanov, O. P. & Gorshkova, T. A. The effect
400 of soil drought on the phloem fiber development in long-fiber flax. *Russ J Plant Physiol*
401 **53**, 656–662 (2006).
- 402 24. Bourmaud, A., Gibaud, M., Lefeuvre, A., Morvan, C. & Baley, C. Influence of the
403 morphology characters of the stem on the lodging resistance of Marilyn flax. *Ind. Crops*
404 *Prod.* **66**, 27–37 (2015).
- 405 25. Bourmaud, A., Beaugrand, J., Shah, D. ., Placet, V. & Baley, C. Towards the design of
406 high-performance plant fibre composites. *Prog. Mater. Sci.* **97**, 347–408 (2018).
- 407 26. Goudenhoft, C., Bourmaud, A. & Baley, C. Study of plant gravitropic response:
408 Exploring the influence of lodging and recovery on the mechanical performances of flax
409 fibers. *Ind. Crops Prod.* **128**, 235–238 (2019).
- 410 27. Hernandez-Estrada, A., Gusovius, H.-J., Müssig, J. & Hughes, M. Assessing the
411 susceptibility of hemp fibre to the formation of dislocations during processing. *Ind. Crops*
412 *Prod.* **85**, 382–388 (2016).
- 413 28. Hughes, M. Defects in natural fibres: their origin, characteristics and implications for
414 natural fibre-reinforced composites. *J. Mater. Sci.* **47**, 599–609 (2012).
- 415 29. Le Duc, A., Vergnes, B. & Budtova, T. Polypropylene/natural fibres composites: Analysis
416 of fibre dimensions after compounding and observations of fibre rupture by rheo-optics.
417 *Compos. Part A Appl. Sci. Manuf.* **42**, 1727–1737 (2011).
- 418 30. Foulk, J., Akin, D. & Dodd, R. Influence of pectinolytic enzymes on retting effectiveness
419 and resultant fiber properties. *BioResources* **3**, 155–169 (2008).
- 420 31. Eder, M., Arnould, O., Dunlop, J. W. C., Hornatowska, J. & Salmen, L. Experimental
421 micromechanical characterisation of wood cell walls. *Wood Sci. Technol.* (2012).

- 422 32. Jäger, A., Bader, T., Hofstetter, K. & Eberhardsteiner, J. The relation between indentation
423 modulus, microfibril angle, and elastic properties of wood cell walls. *Compos. Part A Appl.*
424 *Sci. Manuf.* **42**, 677–685 (2011).
- 425 33. Capron, M. *et al.* Mechanical characterization of developing tension wood fibre wall by
426 atomic force microscopy. in *8th Plant Biomechanics International Conference* 224-225.
427 (2015).
- 428 34. Bader, T. K., de Borst, K., Fackler, K., Ters, T. & Braovac, S. A nano to macroscale study
429 on structure-mechanics relationships of archaeological oak. *J. Cult. Herit.* **14**, 377–388
430 (2013).
- 431 35. Shaw, C. . *Cone Beam Computed Tomography.* (Taylor & Francis Group, 2014).
432
433
434
435
436
437

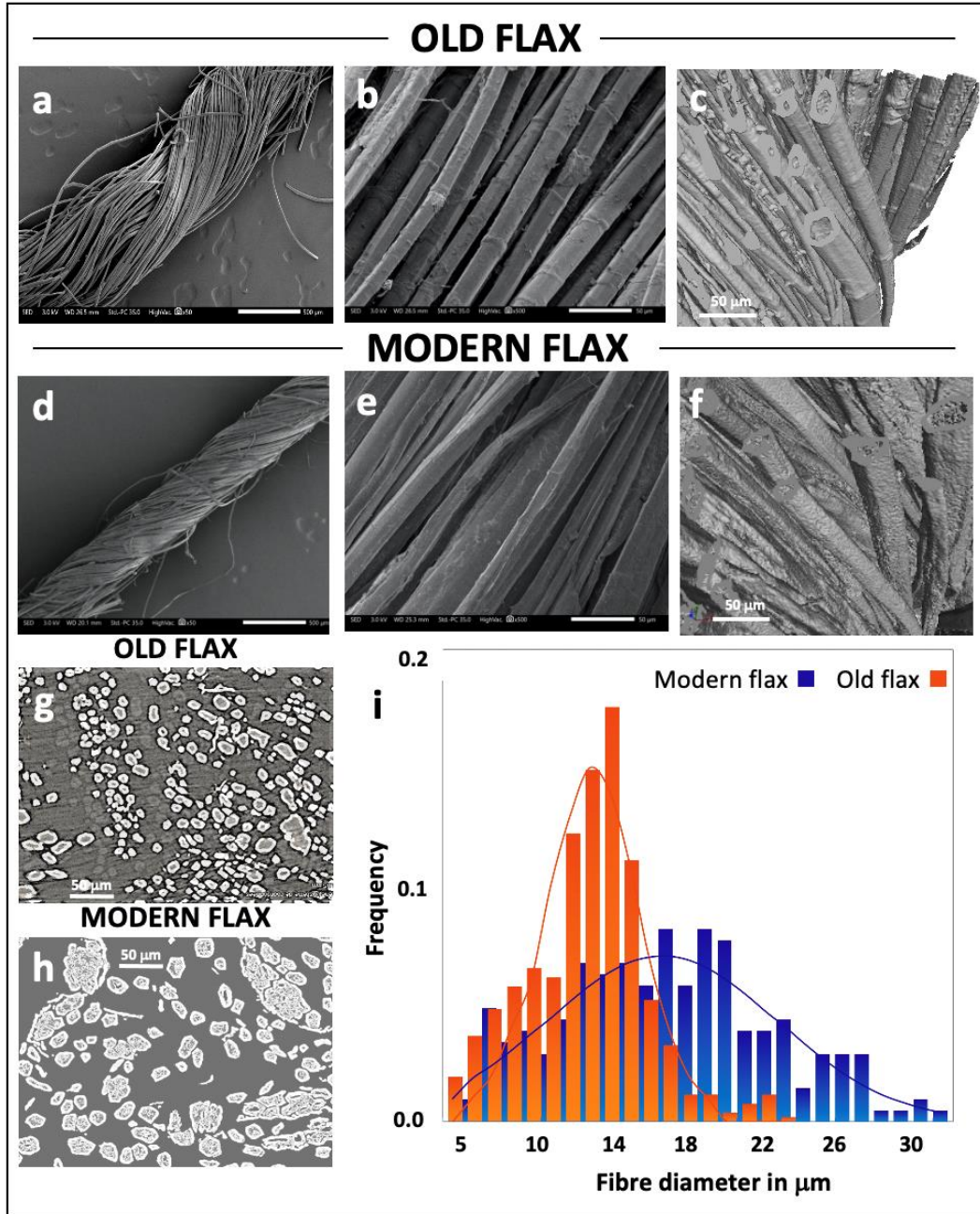


438
439

440 **Fig. 1. Examples of the uses of flax in ancient Egypt.** Child's vest with dyed blue edges, 800-
441 720 or 700-540 BCE (a); Mummy of man with flax agglomerated and stuccoed fabric, 332-30
442 BCE (b); Flax hypocephalus, 305-30 BCE (c); Fragment of flax shroud, 1550-1295 BCE (d);
443 Hairnet cap, AD 5th or 6th century (e); Unspun flax hank, 1420-1230 BCE (f) and Mortuary
444 linen, 2140-1976 BCE (g). Objects c and d are exposed at the British Museum (London-UK); a,
445 b, e, f and g are exposed (b) or in the store room (a, e, f and g) at the Louvre Museum (Paris-F).
446 All images are from the authors' personal collection.

447

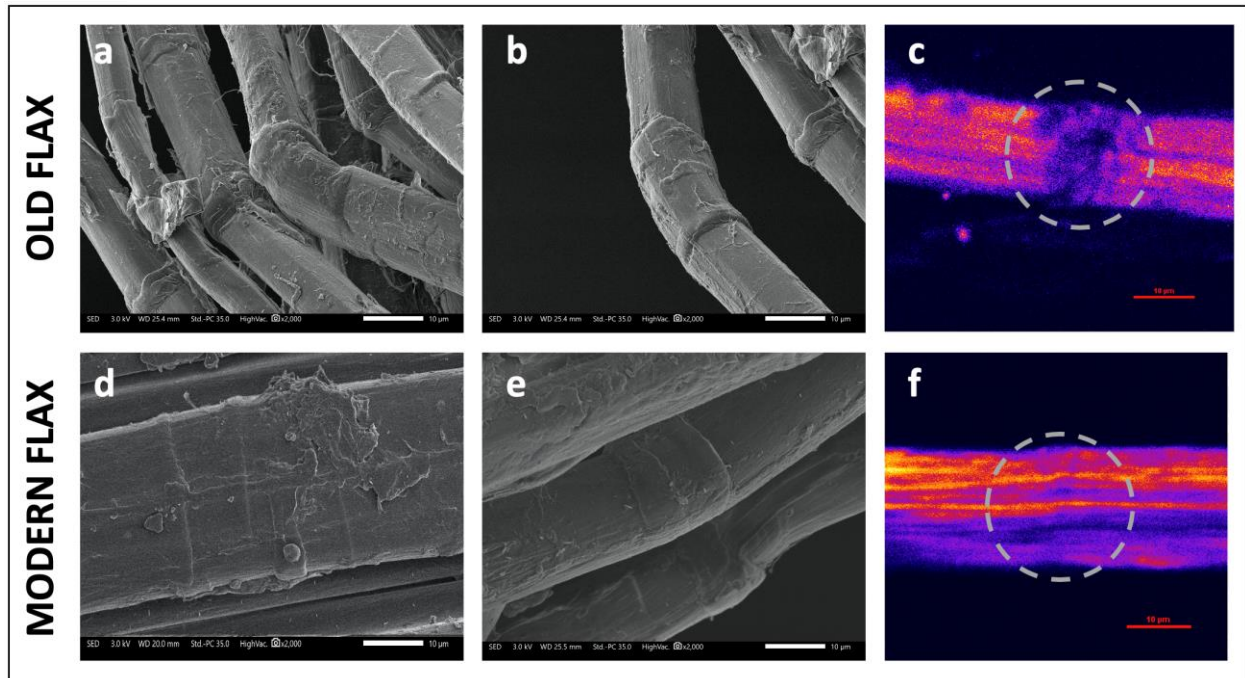
448
449
450
451
452
453
454
455
456
457



458

459 **Fig. 2.** Scanning electronic microscopy and nano-tomography images of modern and 4000-
 460 year-old flax. Overview of yarn (a, d) and fibres within the yarns (b, e); Tomographic overview of
 461 fibres highlighting the larger lumen size for old flax (c, f) and tomographic yarn cross-section
 462 showing the lower diameter of old flax fibres (g, h). Histograms (i) present the distribution of
 463 single fibre diameter for both old and modern flax.

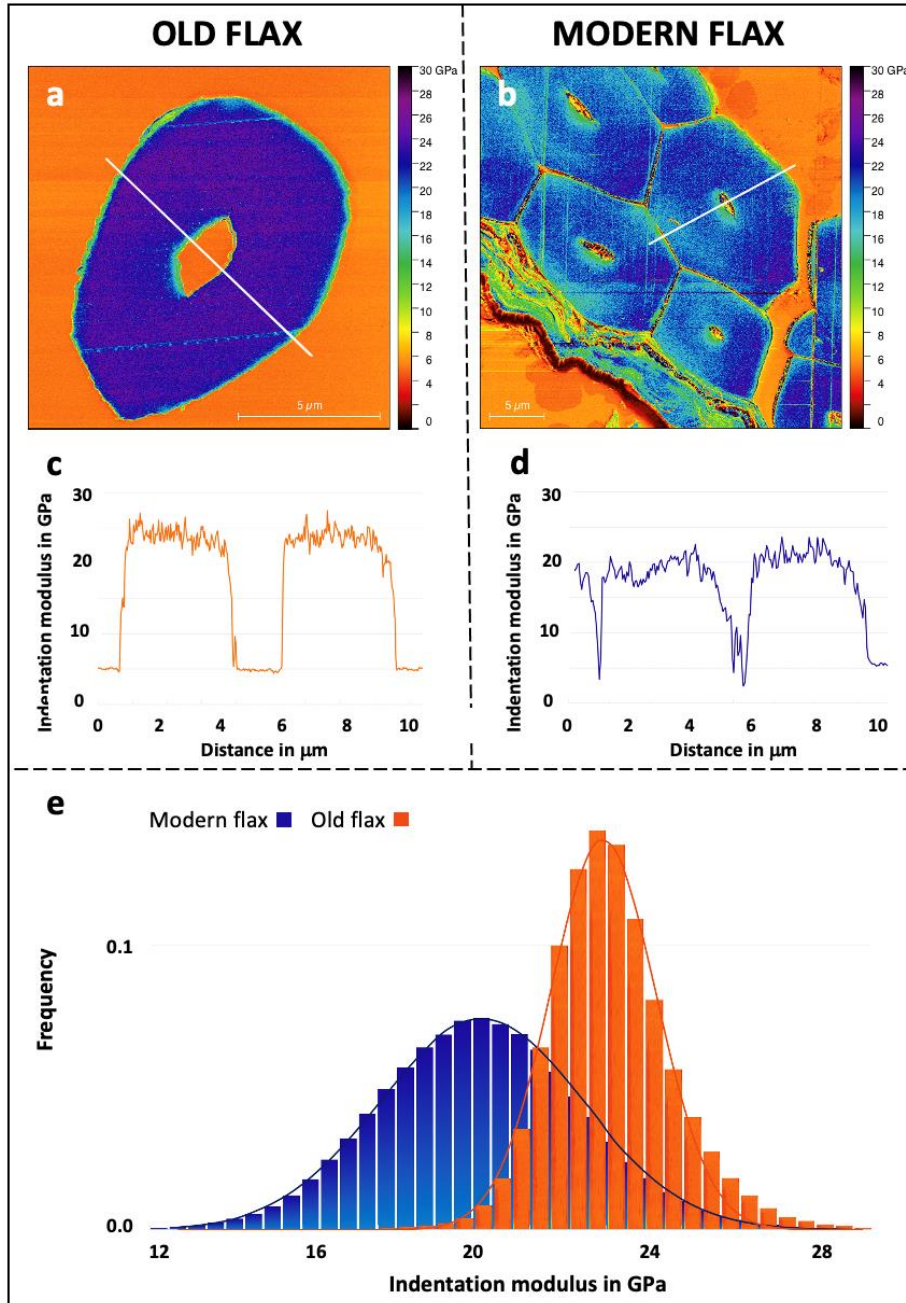
464



465
466

467 **Fig. 3. Focus on kink-band (defect) regions in the fibres.** Scanning electron microscopy
468 images showing differences between kink-bands structure and intensity in old (a, b) and modern
469 (d, e) flax. SHG microscopy observations highlighting the local disorganization of cellulose
470 microfibrils in the kink-band region for old flax (c) compared to modern flax (f). In Figures 3.c
471 and 3.f, kink band region is circled by the dotted grey line.

472



473

474 **Fig. 4. AFM peak force measurements in old and modern flax fibres.** One can notice larger

475 lumen size on old flax fibre (a) and residue of cortical parenchyma on modern flax (b). Figure c

476 and d show the profile of indentation modulus in old (c) and modern (d) flax according to the

477 position on the white line (a and b). Distributions of indentation modulus are shown in (e); they

478 are in good agreement with the preliminary nanoindentation tests performed (Supplementary

479 Tab. 1).